Journal of Biomolecular NMR, **16:** 39–46, 2000.
KLUWER/ESCOM

Determination of $^{h2}J_{NN}$ and $^{h1}J_{HN}$ coupling constants across Watson–Crick base pairs in the *Antennapedia* homeodomain–DNA complex using TROSY

Konstantin Pervushin[a], César Fernández[a], Roland Riek[a], Akira Ono[b], Masatsune Kainosho[b,*] & Kurt Wüthrich[a,*]

[a]*Institut für Molekularbiologie und Biophysik, Eidgenössische Technische Hochschule Hönggerberg, CH-8093 Zürich, Switzerland*

[b]*Department of Chemistry, Faculty of Science, Tokyo Metropolitan University, 1-1 Minamiohsawa, Hachioji, Tokyo 192-03, Japan*

Received 2 September 1999; Accepted 2 December 1999

Key words: hydrogen bonds, nucleic acid structure, scalar coupling, TROSY

Abstract

This paper describes NMR measurements of ^{15}N–^{15}N and ^{1}H–^{15}N scalar couplings across hydrogen bonds in Watson–Crick base pairs, $^{h2}J_{NN}$ and $^{h1}J_{HN}$, in a 17 kDa *Antennapedia* homeodomain–DNA complex. A new NMR experiment is introduced which relies on zero-quantum coherence-based transverse relaxation-optimized spectroscopy (ZQ-TROSY) and enables measurements of $^{h1}J_{HN}$ couplings in larger molecules. The $^{h2}J_{NN}$ and $^{h1}J_{HN}$ couplings open a new avenue for comparative studies of DNA duplexes and other forms of nucleic acids free in solution and in complexes with proteins, drugs or possibly other classes of compounds.

Abbreviations: 2D, two-dimensional; FID, free induction decay; PFG, pulsed field gradient; *Antp*, *Antennapedia*; TROSY, transverse relaxation-optimized spectroscopy; ZQ, zero-quantum.

Introduction

Compared with conventional NMR correlation spectroscopy (Cavanagh et al., 1996), transverse relaxation-optimized ^{15}N–^{1}H correlation spectroscopy ([^{15}N,^{1}H]-TROSY; Pervushin et al., 1997) yields about 70% and 30% reduction of the ^{15}N and ^{1}H linewidths, respectively, in the signals of the guanosine $^{15}N_1$–^{1}H and thymidine $^{15}N_3$–^{1}H imino groups in ^{15}N-labeled DNA (Pervushin et al., 1998c). The reduced TROSY linewidths then allow observation of scalar couplings across base pair hydrogen bonds either by direct measurement in resolved multiplet fine structures (Pervushin et al., 1998c) or in more complex coherence transfer experiments (Dingley and Grzesiek, 1998; Pervushin et al., 1998c). In this paper we report such measurements for a DNA–protein complex, and we compare the $^{h2}J_{NN}$ and $^{h1}J_{HN}$ couplings in the free 14-mer DNA duplex representing the *BS2* operator site (Müller et al., 1988) with the corresponding values measured for the complex of this DNA duplex with the *Antennapedia* homeodomain (Otting et al., 1989; Billeter et al., 1993; Qian et al., 1993; Fernández et al., 1998).

For measurements of $^{h2}J_{NN}$ the previously described experimental scheme (Pervushin et al., 1998c) yielded high quality spectra also for the DNA complex with the *Antp* homeodomain, thus enabling a direct comparison of the free DNA and its protein complex without the need of further method development. In contrast, for the measurement of $^{h1}J_{HN}$ couplings the previously used E.COSY-based approach (Pervushin et al., 1998c) had to be replaced with a novel technique, since for the 17 kDa *Antp* homeodomain–DNA

*To whom correspondence should be addressed. Fax: +41-1-633 11 51 (K.W.); +81-426 77 2525 (M.K.).

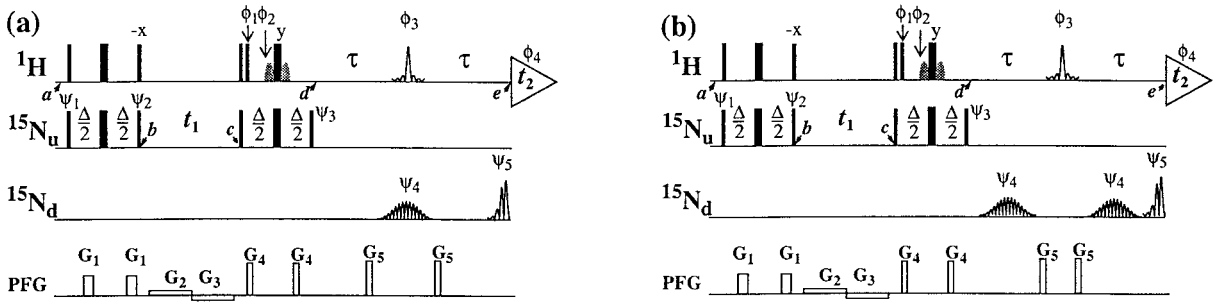

Figure 1. The 2D $^{h1}J_{HN}$-quantitative [^{15}N,^{1}H]-ZQ TROSY experiment used to measure $^{h1}J_{HN}$ scalar coupling constants across hydrogen bonds in Watson–Crick base pairs. For the evaluation of $^{h1}J_{HN}$, a reference spectrum is recorded with scheme (b), where magnetization transfer via $^{h1}J_{HN}$ is suppressed. The actual measurement relies on a difference spectrum obtained by subtraction of a data set measured with scheme (b) from a data set measured with (a) (for details see below). The coupling constants are calculated with Equation 5 from the ratio of the cross peak amplitudes in the reference and difference spectra (see text). In the experimental schemes, narrow and wide bars indicate non-selective 90° and 180° pulses applied at the ^{1}H and the '^{15}N-upfield' (^{15}N$_u$) frequencies, with the carrier offsets placed at 12 ppm and 153 ppm, respectively. After the ψ_3(^{15}N) pulse the ^{15}N carrier is shifted to the '^{15}N downfield' (^{15}N$_d$) frequency at 210 ppm, where the band-selective, shaped ^{15}N pulses on the line marked ^{15}N$_d$ are applied. *a*, *b*, *c*, *d* and *e* indicate time points that are referred to in the text. Water saturation is minimized by keeping the water magnetization along the +z-axis during the entire experiment, which is achieved by the application of the off-resonance water-selective 90° rf-pulses indicated by shaded shapes on the line ^{1}H (Piotto et al., 1992). The delays for the magnetization transfers are $\Delta = 5.4$ ms and $\tau = 40$ ms. The line marked PFG indicates the pulsed magnetic field gradients applied along the z-axis: G$_1$, amplitude 12 G/cm, duration 2 ms; G$_2$, 0.5 G/cm, 0.5 t_1; G$_3$, −0.5 G/cm, 0.5 t_1; G$_4$, 20 G/cm, 1 ms; G$_5$, 23 G/cm, 1 ms. The phases for the rf-pulses are: $\phi_1 = \{x\}$; $\phi_2 = \{-x\}$; $\phi_3 = \{x\}$; $\phi_4 = \{x, -x, -y, y\}$; $\psi_1 = \{-x, x, -y, y\}$; $\psi_2 = \{y, -y, x, -x\}$; $\psi_3 = \{y\}$; $\psi_4 = \{x\}$; $\psi_5 = \{y\}$; x on all pulses without phase specification. The pulse ψ_4 includes a two-band-selective adiabatic inversion ($M_z \rightarrow -M_z$) WURST-2 pulse (Kupče and Wagner, 1995; Kupče and Freeman, 1996) with a duration of 8 ms and $\gamma B_1(\max) = 830$ Hz, which inverts two bands of width 800 Hz each, with the centers separated by 2050 Hz (Figure 2d). The pulse ϕ_3 consists of a refocusing ($M_y \rightarrow -M_y$) RE-BURP pulse (Geen and Freeman, 1991), with a duration of 1.4 ms and $\gamma B_1(\max) = 4.4$ kHz. The pulse ψ_5 consists of an excitation ($M_z \rightarrow M_x$) E-BURP-2 pulse (Geen and Freeman, 1991), with a duration of 1.4 ms and $\gamma B_1(\max) = 3.1$ kHz. For each individual data set recorded with (a) or (b), a complex interferogram is obtained by recording a second FID for each t_1 delay, with $\phi_1 = \{-x\}$, $\phi_2 = \{x\}$, $\phi_4 = \{x, -x, y, -y\}$, and $\psi_3 = \{-y\}$, which results in a phase-sensitive 2D [^{1}H,^{15}N]-correlation spectrum that contains only the slowly relaxing component of the 2D ^{15}N–^{1}H multiplet. For the difference experiment each step in the phase cycle is performed twice, using the experimental schemes (a) and (b), respectively, and then the two FIDs are subtracted. The reference experiment is performed only with the experimental scheme (b). For the data processing we used the procedures of Kay et al. (1992).

complex the broad component of the multiplet, which would be needed as a reference, was beyond detection. To fully benefit from the use of TROSY, only the narrowest component of the ^{15}N–^{1}H multiplets should therefore be used for the $^{h1}J_{HN}$ measurements. We found that this can be achieved by a combination of TROSY and the *J*-quantitative class of experiments (Blake et al., 1992), which enables studies of $^{h1}J_{HN}$ in larger nucleic acid fragments, and in nucleic acid complexes with proteins and other compounds.

Methods

Measurement of $^{h2}J_{NN}$ in the Antp homeodomain–DNA complex

The [^{15}N,^{1}H]-TROSY experiment (Pervushin et al., 1997, 1998a), when applied to the *Antp* homeodomain–DNA complex at 15 °C, yielded sufficiently narrow ^{15}N lines to enable direct extraction of the $^{h2}J_{NN}$ couplings from the in-phase splittings along the ω_1(^{15}N) axis. The $^{h2}J_{NN}$ coupling constants were independently evaluated also from a 2D $^{h2}J_{NN}$-correlation-[^{15}N,^{1}H]-TROSY experiment, which transfers magnetization between the hydrogen-bonded ^{15}N spins via the $^{h2}J_{NN}$ coupling (Figure 1c in Pervushin et al., 1998c).

Measurements of the $^{h1}J_{HN}$ couplings in the Antp homeodomain–DNA complex

For studies of $^{h1}J_{HN}$ couplings we introduce the 2D $^{h1}J_{HN}$-quantitative [^{15}N,^{1}H]-Zero-Quantum-TROSY experiment (Figure 1), which employs the slowly relaxing component of the imino ^{1}H doublet to relay magnetization via $^{h1}J_{HN}$ across the hydrogen bond to the tertiary ^{15}N of the second base in the Watson–Crick base pair. In the following description the density matrix transformations during the experiment are represented in terms of the single-transition basis operators $I_i^{13} = \frac{1}{2}I_i + I_iS_i$ and $I_i^{24} = \frac{1}{2}I_i - I_iS_i$, where *I* and *S* represent the ^{1}H and ^{15}N spins, and *i* stands for 'z', '+' or '−'. The abbreviations $DQ_\pm = I_\pm S_\pm$ and

$ZQ_{\pm} = I_{\mp}S_{\pm}$ are used for double-quantum and zero-quantum operators, respectively. The relevant magnetization transfer pathway is given by Equation 1:

$$\mathrm{u}S_z + \mathrm{v}I_z \rightarrow \frac{\mathrm{u}+\mathrm{v}}{2} ZQ_- \exp[(-R^{ZQ} - i\Omega^{ZQ})t_1] \rightarrow \frac{\mathrm{u}+\mathrm{v}}{2} I_-^{24} \exp[(-R^{24} + i\Omega^{24})t_2] \qquad (1)$$

u and v represent the initial steady-state ^{15}N and ^{1}H magnetizations, respectively; Ω_I and Ω_S are the chemical shifts relative to the carrier frequency of the spins I and S, J is the I–S scalar coupling constant, $\Omega^{ZQ} = \Omega_I - \Omega_S$, $\Omega^{24} = \Omega_I - \pi^1 J_{\mathrm{HN}}$, R^{ZQ} is the relaxation rate of the zero-quantum coherence, and R^{24} is the previously described relaxation rate of the individual single-quantum transition $2 \rightarrow 4$ (Pervushin et al., 1997). For an isolated ^{15}N–^{1}H spin system in the slow tumbling limit, with the rotational correlation time τ_c, these rates are given by Equations 2 and 3:

$$R^{ZQ} = 8/5\tau_c(|\delta_I| - |\delta_S|)^2 \qquad (2)$$

$$R^{24} = 8/5\tau_c(|\mathrm{p}| - |\delta_S|)^2 \qquad (3)$$

The dipole–dipole (DD) coupling constant is $\mathrm{p}^2 = \frac{1}{8}(\gamma_I\gamma_S\hbar/\mathrm{r}_{IS}^3)^2$, and the chemical shift anisotropy (CSA) interactions are $\delta_S^2 = \frac{1}{18}(\omega_S\Delta\sigma_S)^2$ and $\delta_I^2 = \frac{1}{18}(\omega_I\Delta\sigma_I)^2$. γ_I and γ_S are the gyromagnetic ratios of I and S, $\hbar$ is the Planck constant divided by 2π, r_{IS} is the distance between the nuclei S and I, and $\Delta\sigma = \sigma_{zz} - 0.5(\sigma_{xx} + \sigma_{yy})$. The principal values of the ^{15}N CSA tensors in nucleic acid bases have been measured by solid state NMR and their relative orientations have been derived from quantum chemical calculations (Hu et al., 1998). $\Delta\sigma = 110$ ppm for N_1(G) and $\Delta\sigma = 90$ ppm for N_3(T), with the principal axes directed along the H–N bond. Since no experimental data are available for the ^{1}H CSA tensors in nucleic acid bases, the ^{1}H$^{\epsilon 1}$ CSA tensor values of tryptophan, as determined by solid state NMR (Ramamoorthy et al., 1997), were used, with $\Delta\sigma = 12.5$ ppm and the principal axis directed along the H–N bond. Based on this information we assume for simplicity that the angle between the directions of the principal axes of the chemical shift tensors of the spins S and I and the N–H bond is zero (for a treatment of non-zero angles and non-symmetrical CSA tensors see Pervushin et al., 1998a).

As indicated in Equation 1 the sensitivity of the experiment is enhanced by the use of both the ^{1}H and ^{15}N steady-state magnetizations (Pervushin et al., 1998a,b). The 2D [^{15}N,^{1}H]-ZQ-TROSY scheme used between the time points *a* and *d* (Figure 1) has recently also been used in TROSY-NOESY experiments, and has been described in detail in this context (Pervushin et al., 1999). Between the time points *d* and *e* the TROSY ^{1}H multiplet component represented by the I_-^{24} operator is used to transfer magnetization to the tertiary nitrogen across the hydrogen bond, using the $^{h1}J_{\mathrm{HN}}$ coupling. Due to the small values of the $^{h1}J_{\mathrm{HN}}$ coupling constants (Pervushin et al., 1998c) long delays τ have to be employed (see caption to Figure 1), so that the use of TROSY is essential during this polarization transfer period. To maintain the TROSY effect the band-selective inversion and excitation of the tertiary ^{15}N spins should be achieved with minimal perturbation of the ^{15}N spins of the imino groups (see Figure 2). In the experimental scheme of Figure 1a, a fraction of the I_-^{24} magnetization (K in Equation 4) is transferred to the tertiary ^{15}N spin, and

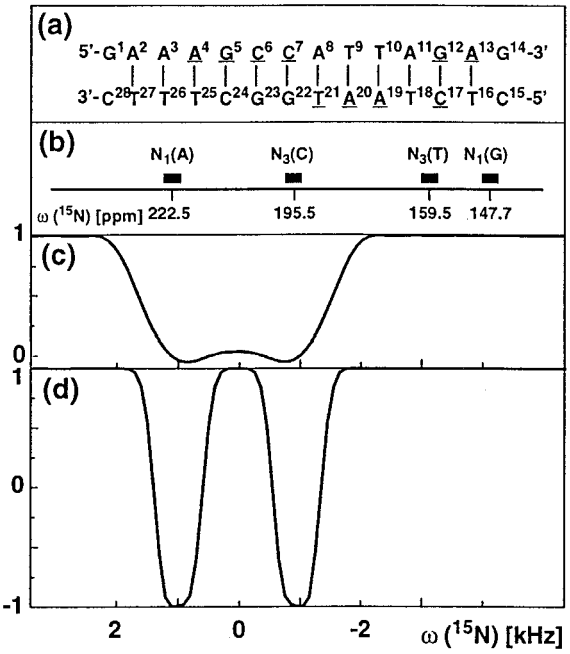

Figure 2. (a) DNA duplex used for this study, with numeration of the individual nucleotides. Underlined letters identify the nucleotides that contain ^{15}N in the partially labeled duplex (see text). Vertical lines connect the bases between which $^{h2}J_{\mathrm{NN}}$ and $^{h1}J_{\mathrm{HN}}$ were observed. (b) ^{15}N chemical shifts of N_1(G), N_3(T), N_3(C) and N_1(A) in the DNA duplex of (a). The spread of the shifts among the non-terminal bases of the duplex free in solution is shown as a horizontal bar above the chemical shift scale. (c) Excitation profile of the E-BURP-2 pulse (Geen and Freeman, 1991) calculated with the parameters used in the experimental scheme of Figure 1. (d) Inversion profile of the WURST-2 pulse (Kupče and Wagner, 1995; Kupče and Freeman, 1996) calculated with the parameters used in the experimental scheme of Figure 1.

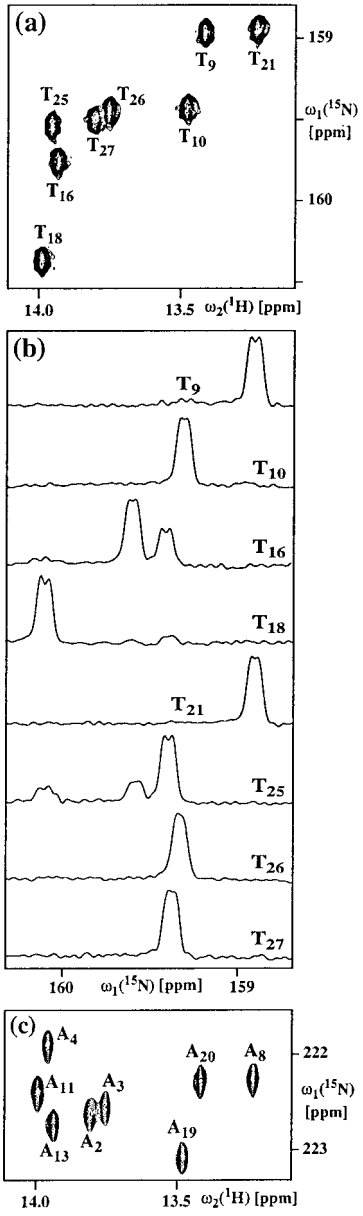

Figure 3. NMR observation of scalar ^{15}N–^{15}N couplings across hydrogen bonds, $^{h2}J_{NN}$, in the *Antp* homeodomain–DNA complex. (a) Contour plot from a [^{15}N,^{1}H]-TROSY spectrum of the uniformly ^{13}C,^{15}N-labeled DNA duplex of Figure 2a in the complex with the *Antp* homeodomain, showing the signals of the A=T base pairs. (b) Cross sections along $\omega_1(^{15}N)$ through the individual cross peaks in spectrum (a). 256 complex t_1 points were acquired, with $t_{1max} = 34$ ms and $t_{2max} = 51$ ms, resulting in 2.5 h of measuring time. (c) Contour plot from a $^{h2}J_{NN}$-correlation-[^{15}N,^{1}H]-TROSY spectrum, showing the relayed [$^{15}N_1$(A),$^{1}H_3$(T)] cross peaks of the A=T base pairs. The spectra were recorded on a Bruker DRX750 spectrometer equipped with a ^{1}H-{^{13}C,^{15}N} triple-resonance probehead (*Antp* homeodomain–DNA complex concentration = 1 mM, solvent 95% H_2O/5% D_2O, pH = 6.0, T = 15 °C). 128 complex t_1 points were acquired, with $t_{1max} = 14$ ms and $t_{2max} = 51$ ms, resulting in 9 h of measuring time.

with the last ^{15}N pulse this magnetization is converted to unobservable multiple-quantum coherence:

$$\begin{aligned} I_-^{24} \rightarrow \{&I_-^{24} K_y \sin[\pi^{h1} J_{HN}(2\tau + (\lambda_W - 1)W \\ &+(\lambda_B - 1)B)] \\ &+I_-^{24} \cos[\pi^{h1} J_{HN}(2\tau + (\lambda_W - 1)W \\ &+(\lambda_B - 1)B)]\} \exp[-R^{24} 2\tau], \end{aligned} \quad (4)$$

W and B stand for the duration of the WURST-2 and E-BURP-2 pulses, respectively, λ_W and λ_B are the effective J coupling scaling factors ($J_{eff} = \lambda J$; Levitt et al., 1983; Kupče et al., 1998) for the WURST-2 and E-BURP-2 pulses, respectively, which relate the effective coupling constant to the unperturbed J coupling. The values of the scaling factors for the ψ_4 and ψ_5 pulse shapes and durations of Figure 1, $\lambda_W = 0.37$ and $\lambda_B = 0.52$, have been calculated by numerical integration of the Liouville-von-Neuman equation for the density operator (Sørensen et al., 1983). In the experimental scheme of Figure 1b the magnetization transfer via $^{h1}J_{HN}$ is suppressed by application of two ψ_4 pulses in the middle of each of the two transfer delays τ. To obtain the desired difference spectrum the experimental schemes of Figure 1, a and b, are used in an interleaved manner, and the two spectra thus obtained are then subtracted (see also the caption to Figure 1).

To properly account for transverse relaxation, a reference experiment without magnetization transfer via the $^{h1}J_{HN}$ scalar couplings was recorded with the use of the scheme of Figure 1b. The coupling constants were then calculated from the ratios of the signal amplitudes, A, in the aforementioned difference spectrum, A^{dif}, and this reference spectrum, A^{ref}, according to Equation 5:

$$\begin{aligned} A^{dif}/A^{ref} = &(1 - \cos\{\pi^{h1} J_{HN}[2\tau + (\lambda_W - 1)W \\ &+(\lambda_B - 1)B]\}) \sqrt{\frac{NS^{dif}}{NS^{ref}}} \end{aligned} \quad (5)$$

NS^{dif} and NS^{ref} are the numbers of scans used to record the difference spectrum and the reference spectrum, respectively. The standard deviations of the resulting scalar coupling constants were calculated by the error propagation method, where the rmsd of the noise in the spectrum was used as the uncertainty of the experimental peak amplitude.

Two features of the experimental schemes of Figure 1 deserve special comments. First, cross-correlated relaxation due to interference between the imino proton CSA and ^{15}N–$^{1}H^N$ DD coupling across the hydrogen bond could in principle affect the peak

Table 1. Values and standard deviations of the ^{15}N–^{1}H scalar spin–spin couplings across hydrogen bonds, $^{h2}J_{HN}$, in Watson–Crick base pairs of a 14-mer DNA duplex free in solution and in a complex with the *Antp* homeodomain

Nucleotide (see Figure 2)	$^{h2}J_{HN}$ (Hz)	
	Free DNA	Complex
T^{9}	6.7 ± 0.1	6.6 ± 0.2
T^{10}	7.0 ± 0.1	7.2 ± 0.2
T^{16}	6.5 ± 0.1	6.7 ± 0.2
T^{18}	6.8 ± 0.1	7.2 ± 0.2
T^{21}	6.5 ± 0.1	6.5 ± 0.2
T^{25}	7.0 ± 0.1	7.1 ± 0.2
T^{26}	6.9 ± 0.1	6.4 ± 0.2
T^{27}	7.0 ± 0.1	6.9 ± 0.2
G^{5}	6.0 ± 0.1	6.5 ± 0.2
G^{12}	6.3 ± 0.1	6.2 ± 0.2
G^{22}	6.5 ± 0.1	6.4 ± 0.2
G^{23}	6.4 ± 0.1	6.2 ± 0.2

[a]Data from Pervushin et al. (1998c).

amplitudes from which the $^{h1}J_{HN}$ values are derived with Equation 5. Therefore, care was taken in the schemes of Figure 1 to suppress possible effects from cross-correlated relaxation in both experiments (a) and (b) by proper positioning of the adiabatic inversion pulses ψ_4. Second, the evolution of the magnetization due to the homonuclear scalar couplings $^{5}J_{H3H7}$ and $^{5}J_{H3H6}$ in thymine, and $^{4}J_{H1H2}$ and possibly $^{6}J_{H1H8}$ in guanine (approximately 1 Hz) during the long delay 2τ, which is needed for the magnetization transfer via $^{h1}J_{HN}$, is refocused by the application of the $^{1}H^{N}$-selective RE-BURP pulse. A comparison with an otherwise identical scheme in which the selective ϕ_3-pulse of Figure 1 was replaced by a non-selective $180°(^{1}H)$ pulse showed that a sensitivity gain of about 30% was achieved by selective refocusing of these couplings (data not shown).

Results and discussion

The structure of the DNA duplex used for this study (Figure 2a) corresponds to a minimal fragment of the *BS2* operator site that is recognized by the *Antp* and *fushi tarazu* homeodomains (Müller et al., 1988). The synthesis of the uniformly ^{13}C,^{15}N-labeled duplex, which yields $^{15}N_1$–^{1}H-correlation cross peaks for all but the terminal base pairs, and the partially labeled duplex with isotope labels only on the underlined nucleotides (Figure 2a), which yields ^{15}N–^{1}H-correlation peaks for G^{5}, G^{12} and T^{21}, was described elsewhere (Fernández et al., 1998). In the protein complex the uniformly labeled DNA was bound to a uniformly ^{15}N-labeled 69-residue polypeptide construct containing the *Antp* homeodomain in positions 1–60 (Müller et al., 1988). For the DNA duplex of Figure 2a free in solution the $^{h2}J_{NN}$ couplings were previously obtained (Pervushin et al., 1998c) from the resolved fine structures in 2D [^{15}N,^{1}H]-TROSY spectra using inverse Fourier transformation of the in-phase doublets, where the standard deviations given in Table 1 were estimated from the quality of the time-domain fitting (Szyperski et al., 1992). Independently, the values of the $^{h2}J_{NN}$ coupling constants were verified from the magnetization transfer efficiencies in a 2D $^{h2}J_{NN}$-correlation-[^{15}N, ^{1}H]-TROSY experiment. Using the same experiments with the *Antp* homeodomain–DNA complex (Figure 3) yielded the corresponding data for the complex (Table 1). The $^{h2}J_{NN}$ couplings observed for the DNA free in solution and in the *Antp* homeodomain complex are very similar, which can be rationalized by the overall very small conformational changes observed in this DNA duplex upon binding to the *Antp* homeodomain (Billeter et al., 1993; Fraenkel and Pabo, 1998; Fernández et al., 1999). It also appears that the $^{h2}J_{NN}$ couplings are not very sensitive to certain variations in the DNA conformation that are, for example, implicated by small chemical shift differences (Fernández et al., 1998) and appear to be manifested also in variations of the $^{h1}J_{HN}$ values (see below). The principal result of the present study of $^{h2}J_{NN}$ couplings is the demonstration that this parameter can readily be measured in structures with high molecular weights. This will be of special interest for studies of supramolecular assemblies containing distorted DNA structures, for example, with individual bases flipped out of a double-helical DNA, or with unwinding of a DNA duplex due to protein–DNA contacts. It remains to be seen, from studies of systems where complexation induces more important changes of the DNA conformation than in the *Antp* homeodomain complex, whether $^{h2}J_{NN}$ values can further be related to more subtle DNA conformational changes than fraying of the base pairs (Pervushin et al., 1998c) or complete breakage of base pairing.

For the measurements of $^{h1}J_{HN}$ the experimental scheme of Figure 1, with the adjustments of the shaped pulses ψ_4 and ψ_5 based on the data in Figure 2b and the calculations in Figure 2, c and d, was first applied

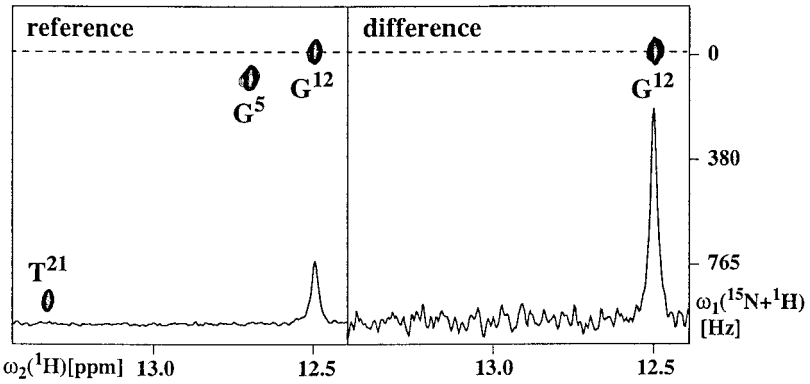

Figure 4. Reference spectrum recorded with the scheme of Figure 1b and difference 2D [^{1}H,^{15}N]-correlation spectrum recorded using both experimental schemes of Figure 1 (see text) for the partially ^{15}N-labeled DNA duplex of Figure 2a. In the contour plot of the reference spectrum the signals of the three labeled G and T nucleotides (Figure 2a) are seen, of which only G^{12} is hydrogen-bonded to a labeled base. The 1D slices along $\omega_2(^1\mathrm{H})$ taken at the position of the broken line, which were used to calculate the $^{h1}J_{HN}$ coupling constants, are shown as insets (DNA duplex concentration = 2.5 mM, solvent 95% H_2O/5% D_2O, pH = 6.0, T = 15 °C, ^{1}H frequency = 750 MHz). For both spectra 32 complex t_1 points were acquired, with t_{1max} = 3.84 ms and t_{2max} = 51 ms. For the reference spectrum, 192 scans per t_1 increment were accumulated, resulting in 4.1 h of measuring time. The number of scans for the difference spectrum was 1216, with a total measuring time of 25.9 h.

with the DNA duplex of Figure 2a free in solution. To unambiguously identify the origin of the signals in the difference spectrum, an experiment was also recorded for the partially ^{15}N-labeled duplex, where either none, one or both nucleotides in the individual Watson–Crick base pairs are ^{15}N-labeled (Figure 2a). As expected, only the $^{15}N_1$–^{1}H-correlation peak of G^{12} was observed in the difference spectrum, while the cross peaks of G^5 and T^{21} are only seen in [^{15}N,^{1}H]-TROSY, since the base-paired nucleotides C^{24} and A^8 are not ^{15}N-labeled. These control experiments thus provide direct evidence that the cross peaks in the difference spectra of the experiment of Figure 1 are indeed due to the $^{h1}J_{HN}$ couplings.

Comparison of the $^{h1}J_{HN}$ values measured with the experiment of Figure 1 (Table 2) with the corresponding data obtained using an E.COSY-based approach (Pervushin et al., 1998c) shows quite good agreement for the G≡C base pairs, whereas the results obtained for the A=T base pairs are more widely different, with T^9 and T^{21} showing differences extending slightly beyond the standard deviations. These differences are apparently due primarily to the fact that the resonances of some A=T base pairs in the free DNA duplex are somewhat broadened, which also caused the large standard deviations for some of the measurements in Table 2.

Table 2 further compares the $^{h1}J_{HN}$ coupling constants measured for the DNA duplex in free form and in the homeodomain complex. Significant differences between corresponding $^{h1}J_{HN}$ couplings are observed for T^9, T^{21}, T^{25}, T^{26}, G^{12}, G^{22} and G^{23}. For these residues, larger values of the $^{h1}J_{HN}$ couplings are observed for the homeodomain complex, which might imply subtle changes in the DNA duplex structure upon complex formation, with the tendency to decrease the hydrogen bond distances from N to HN for some nucleotides involved in protein binding in the complex. A more precise structural interpretation of the $^{h1}J_{HN}$ data, which should then also include an

Table 2. Values and standard deviations of the ^{15}N–^{1}H scalar spin–spin couplings across hydrogen bonds, $^{h1}J_{HN}$, in Watson–Crick base pairs of a 14-mer DNA duplex free in solution and in a complex with the *Antp* homeodomain

Nucleotide (see Figure 2)	$^{h1}J_{HN}$ (Hz)	
	Free DNA	Complex
T^9	2.2 ± 0.4	3.0 ± 0.2
T^{10}	2.7 ± 0.7	2.7 ± 0.3
T^{16}	2.4 ± 0.8	3.0 ± 0.4
T^{18}	3.1 ± 0.9	3.1 ± 0.3
T^{21}	2.4 ± 0.4	3.1 ± 0.2
T^{25}	2.3 ± 0.2	3.2 ± 0.2
T^{26}	2.4 ± 0.3	3.0 ± 0.3
T^{27}	2.7 ± 0.8	3.0 ± 0.8
G^5	3.1 ± 0.1	3.3 ± 0.6
G^{12}	3.0 ± 0.2	3.9 ± 0.4
G^{22}	2.7 ± 0.3	3.9 ± 0.6
G^{23}	3.0 ± 0.2	4.1 ± 0.6

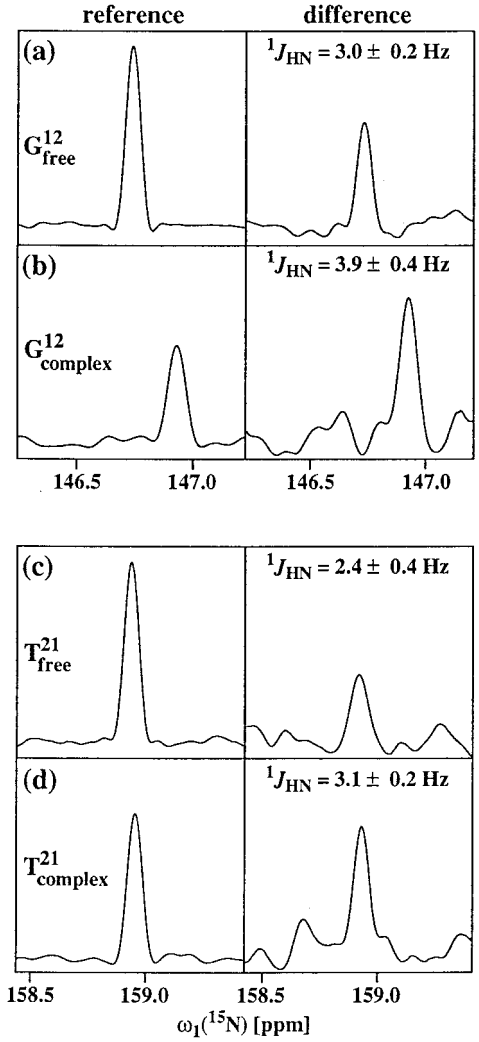

Figure 5. 1D cross sections along $\omega_1(^{15}N)$ taken at the chemical shifts of $N_1(G^{12})$ and $N_3(T^{21})$, which were used to calculate the $^{h1}J_{HN}$ coupling constants for the base pairs containing these nucleotides in the uniformly ^{15}N-labeled DNA duplex of Figure 2a free in solution (a and c) or in the complex with the *Antp* homeodomain (b and d). The acquisition parameters and the experimental conditions are identical to those described in Figure 4, except that 2368 scans per t_1 increment were accumulated for the difference spectrum of the *Antp* homeodomain–DNA complex, resulting in 50.5 h of measuring time. The average values and standard deviations of the calculated $^{h1}J_{HN}$ coupling constants are shown in the inset. Both NMR samples contained a 1 mM solute concentration (solvent 95% H_2O/5% D_2O, pH = 6.0, T = 15 °C).

explanation of the apparent insensitivity of the $^{h2}J_{NN}$ values to the same structure variations (Table 1), has to await the establishment of rational criteria relating scalar couplings across hydrogen bonds with distinct conformational features of nucleic acids (Dingley et al., 1999).

This paper demonstrates that with the use of the experiment of Figure 1, $^{h1}J_{HN}$ couplings in DNA can be measured in structures of molecular weights up to at least 20 to 30 kDa. However, the present results also show that the precision of the $^{h1}J_{HN}$ measurements is critically dependent on the signal-to-noise ratio in the difference spectrum of the 2D $^{h1}J_{HN}$-quantitative [^{15}N,^1H]-ZQ-TROSY experiment (Figures 4 and 5). Equation 4 shows that the transverse relaxation during the long polarization transfer delays τ is the major factor that limits the application of the *J*-quantitative approach for measurements of small coupling constants in large molecules (Blake et al., 1992a, b). The use of TROSY enables to expand the size of the structures for which such couplings can be measured and analyzed, but even slight line broadening by mechanisms that are not affected by TROSY can greatly reduce the precision of the measurements, as observed for some A=T base pairs in the free form of the DNA duplex of Figure 2a (Table 2). Although there are indications that the $^{h1}J_{HN}$ values might be quite sensitive to subtle changes in DNA conformation (see Table 2), the ease with which $^{h2}J_{NN}$ can be obtained for larger structures (Figure 3) might make this latter parameter particularly valuable for studies of systems including DNA molecules with major distortions relative to canonical duplex structures.

Acknowledgements

Financial support was obtained from the Schweizerischer Nationalfonds (Project 31. 49047.96), from the ETH Zürich for a special grant within the framework of the Swiss-Japanese R&D Roundtable Collaboration, and by CREST (Core Research for Evolutional Science and Technology) of the Japan Science and Technology Corporation (JST). We thank Mrs. M. Geier for the careful processing of the manuscript.

References

Billeter, M., Qian, Y.Q., Otting, G., Müller, M., Gehring, W.J. and Wüthrich, K. (1993) *J. Mol. Biol.*, **234**, 1084–1093.

Blake, P.R., Lee, B., Summers, M.F., Adams, M.W.W., Park, J.B., Zhou, Z.H. and Bax, A. (1992) *J. Biomol. NMR*, **2**, 527–533.

Blake, P.R., Park, J.B., Adams, M.W.W. and Summers, M.F. (1992) *J. Am. Chem. Soc.*, **114**, 4931–4933.

Cavanagh, J. and Rance, M. (1993) *Annu. Rep. NMR Spectrosc.*, **27**, 1–58.

Dingley, A.J. and Grzesiek, S. (1998) *J. Am. Chem. Soc.*, **120**, 8293–8297.

Dingley, A.J., Masse, J.E., Peterson, R.D., Barfield, M., Feigon, J. and Grzesiek, S. (1999) *J. Am. Chem. Soc.*, **121**, 6019–6027.
Fernández, C., Szyperski, T., Ono, A., Iwai, H., Tate, S., Kainosho, M. and Wüthrich, K. (1998) *J. Biomol. NMR*, **12**, 25–37.
Fernández, C., Szyperski, T., Ono, A., Iwai, H., Tate, S., Kainosho, M. and Wüthrich, K. (1999) *J. Mol. Biol.*, **292**, 609–617.
Fraenkel, E. and Pabo, C.O. (1998) *Nat. Struct. Biol.*, **5**, 692–697.
Geen, H. and Freeman, R. (1991) *J. Magn. Reson.*, **93**, 93–141.
Hu, J.Z., Facelli, J.C., Alderman, D.W., Pugmire, R.J. and Grant, D.M. (1998) *J. Am. Chem. Soc.*, **120**, 9863–9869.
Kay, L.E., Keifer, P. and Saarinen, T. (1992) *J. Am. Chem. Soc.*, **114**, 10663–10665.
Kupče, E. and Freeman, R. (1996) *J. Magn. Reson.*, **A118**, 299–303.
Kupče, E. and Wagner, G. (1995) *J. Magn. Reson.*, **B109**, 329–333.
Kupče, E., Schmidt, P., Rance, M. and Wagner, G. (1998) *J. Magn. Reson.*, **135**, 361–367.
Levitt, M., Freeman, R. and Frenkiel, T. (1983) *Adv. Magn. Reson.*, **11**, 47–110.
Müller, M., Affolter, M., Leupin, W., Otting, G., Wüthrich, K. and Gehring, W.J. (1988) *EMBO J.*, **7**, 4299–4304.
Palmer III, A.G., Cavanagh, J., Wright, P.E. and Rance, M. (1991) *J. Magn. Reson.*, **93**, 151–170.
Pervushin, K., Riek, R., Wider, G. and Wüthrich, K. (1997) *Proc. Natl. Acad. Sci. USA*, **94**, 12366–12371.
Pervushin, K., Riek, R., Wider, G. and Wüthrich, K. (1998a) *J. Am. Chem. Soc.*, **120**, 6394–6400.
Pervushin, K., Wider, G. and Wüthrich, K. (1998b) *J. Biomol. NMR*, **12**, 345–348.
Pervushin, K., Ono, A., Fernández, C., Szyperski, T., Kainosho, M. and Wüthrich, K. (1998c) *Proc. Natl. Acad. Sci. USA*, **95**, 14147–14151.
Pervushin, K., Riek, R., Wider, G. and Wüthrich, K. (1999) *Proc. Natl. Acad. Sci. USA*, **96**, 9607–9612.
Piotto, M., Saudek, V. and Sklenar, V.J. (1992) *J. Biomol. NMR*, **2**, 661–665.
Qian, Y.Q., Otting, G. and Wüthrich, K. (1993) *J. Am. Chem. Soc.*, **115**, 1189–1190.
Ramamoorthy, A., Wu, C.H. and Opella, S.J. (1997) *J. Am. Chem. Soc.*, **119**, 10479–10486.
Sørensen, O.W., Eich, G.W., Levitt, M.H., Bodenhausen, G. and Ernst, R.R. (1983) *Progr. NMR Spectrosc.*, **16**, 163–192.
Szyperski, T., Güntert, P., Otting, G. and Wüthrich, K. (1992) *J. Magn. Reson.*, **99**, 552–560.
Szyperski, T., Ono, A., Fernández, C., Kainosho, M. and Wüthrich, K. (1998) *J. Am. Chem. Soc.*, **120**, 821–822.